Measuring Tissue Elastic Properties Using Physics Based Neural Networks

Aishwarya Mallampati
School of Electrical Engineering and Computer Science
The Pennsylvania State University
University Park, PA
abm6404@psu.edu

Mohamed Almekkawy
School of Electrical Engineering and Computer Science
The Pennsylvania State University
University Park, PA
mka9@psu.edu

2021 IEEE UFFC Latin America Ultrasonics Symposium (LAUS) | 978-1-6654-4359-3/21/$31.00 ©2021 IEEE | DOI: 10.1109/LAUS53676.2021.9639231

***Abstract*—Ultrasound elastography is a non-invasive and low-cost imaging technique that is used to detect abnormalities in soft tissues. Elastography detects solid tumors from healthy tissues by observing changes in elasticity of tissues on application of force. Reconstruction of initial tissue modulus distribution based on measured displacement/strain fields is called an inverse elasticity problem which has a wide range of applications in medical diagnosis. This paper tries to measure the elastic properties of tissues using Physics-Informed Neural Networks (PINNs). The input data consists of pre-compression and post-compression images of a phantom. Displacement and strain fields are computed from input data which are fed to our PINN model. The PINN model consists of five independent feed-forward neural networks. The model is trained using a loss function that incorporates physics laws based on linear elasticity along with the input data. Lame constants (λ and μ) are considered as network parameters that change during the training phase. The ground truth λ value is 920 kPa whereas the value predicted by the model is 925.319 kPa. The results indicated that that PINNs can solve inverse problems in the domain of ultrasound elastography.**

***Index Terms*—Elastography, Ultrasound, Artificial Neural Networks, Deep Learning, Physics-Informed Neural Networks, Linear elasticity**

I. Introduction

Traditionally, physicians use palpation to detect tumors and other diseases by observing changes in mechanical properties of soft tissues [1]. Palpation is a highly subjective method which largely depends on physician's experience [2]. An accurate assessment of the elastic properties of soft tissues can significantly help in the objective diagnosis of tumors and other diseases. Measuring tissue elastic properties is a difficult and time-consuming task. Various studies focused on modelling complex elasticity properties and a wide variety of biomedical models are used because of their high accuracy [3], [4]. However, these techniques are considered complex and the correctness of the solution depends on the accuracy of the tissue geometry modeling. When the deformation shape function is approximated, Takács et al. [5] employed curve fitting to estimate mechanical parameters and achieved good estimation of reaction force. Finite-Element Method (FEM) is also a powerful technique to simulate mechanical and physical properties of elastic objects [6]. FEM techniques are considered more accurate than modeling methods. For example, Mcgrath et al. [7] has assumed that soft tissues are linearly elastic and used this property to update Young's modulus of soft tissues iteratively. Optimization algorithms are also widely used to calculate properties of soft tissues [8], [9].

Some of the recent studies directly use images to measure elastic parameters of soft bodies. Magnetic Resonance Imaging (MRI) was used to estimate passive mechanical properties in myocardial infarction [10]. Accurate estimation of displacement and strain fields from ultrasound images is very important to predict the elastic properties of soft tissues. Speckle tracking are well known methods in ultrasound imaging to estimate the motion of each pixel from consecutive frames. Speckle tracking can be performed using iterative projection methods [11] and also by applying Riesz transform [12], [13]. Correlation and interpolation [14]–[16] techniques are also widely used for speckle tracking. Motion tracking methods using deep learning [17]–[21] are also becoming quite popular in the field of ultrasound elastography.

In recent years, Artificial Neural Networks(ANNs) are widely used to solve problems in various fields, such as image classification, handwriting recognition, speech recognition, computer vision and medical imaging. The performance of search engines, autonomous driving, e-commerce and photography improved drastically due to these ANN appoaches [22]–[24]. In conjunction with large deep learning frameworks, a new class of ANNs called Physics-Informed Neural Networks (PINNs) [25] is introduced to solve forward and inverse problems involving Partial Differential Equations (PDEs). The main idea behind the development of PINNs is to embed the equations that govern the physics of the system into the network model. The training of PINNs is performed with a cost function that, in addition to data, includes the governing equations, initial and boundary conditions. PINNs have been used to solve forward and inverse problems in fluid mechanics [26], solid mechanics [27], biomaterials [28] and optics [29] etc. There are also other PINN variants that can be used to solve fractional PDEs [30], stochastic PDEs [31], and for introducing uncertainty by combining Bayesian neural networks [32].

Availability of advanced algorithms and machine-learning software are considered as the main reasons for the success of all these studies. From the results of all these works, it has

been observed that PINNs played a very important role in integrating physics laws into deep learning frameworks. The training of the PINN models converges on very sparse data set as networks utilize data as implicit knowledge and physics constraints as explicit knowledge during training. In this paper, PINNs are used to solve the inverse problem in the field of elastography: given the measured displacement data of soft tissue under quasi-static loading, the main goal is to estimate the lame parameters of the material using PINNs. SciANN library [33] has been used, in this paper, to build the model.

II. Materials and Methods

A. Data

The input data is the pre and post compression images of the phantom. This dataset was introduced by Rivaz et al. [34]. From Fig. 1, it can be observed that the input data has lesion and background information. The Young's elasticity modulus of lesion is 56 kPa and of the background is 33 kPa. The λ and μ values are calculated using the linear-elasticity equation (1). So, given pre and post compression images, the lateral and axial displacement are computed using AM2D algorithm [34]. Displacement is used to compute strain. Stress fields are computed using displacement, strain and the lame constants. All this pre-processing is performed in MATLAB. The dimension of the input images is 1500 $\times$ 400. Poisson's ratio of the material is 0.49.

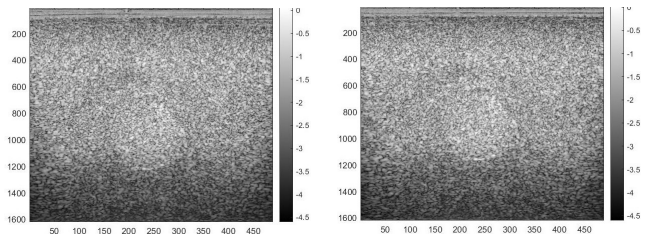

(a) (b)

Fig. 1. Images of the phantom: (a) Pre-compression (b) Post-compression.

TABLE I
PROPERTIES OF THE USED PHANTOM

Material	Young's Elasticity Modulus (kPa)	λ (kPa)	μ
Lesion	56	920.80	18.791e3
Background	33	542.6	11.07e3

B. SciANN Framework

SciANN library [33] is used to build the PINN model in this paper. It is a high-level artificial neural networks interface, written in Python using Keras and Tensorflow backends. It is developed with a focus on enabling fast experimentation with different network architectures and with emphasis on scientific computations, physics informed deep learning, and inversion.

C. PINN

1) Linear Elasticity: Linear elasticity is a mathematical model which explains the stress-strain relationship in solid objects when some force is applied on them.

$$\begin{aligned}\sigma_{ij} =& \lambda\delta_{ij}\varepsilon_{kk} + 2\mu\varepsilon_{ij} \\ =& \lambda\delta_{ij}u_{k,k} + \mu(u_{i,j} + u_{j,i})\end{aligned} \tag{1}$$

where, σ_{ij} is the Cauchy stress tensor. For the two-dimensional problems considered here: $i, j = x, y$, respectively. We used the summation convention and the subscript denotes partial derivative. u_i represents the displacements, ε_{ij} is the infinitesimal stress tensor and δ_{ij} is the Kronecker delta. λ and μ are the quantities to be inferred using PINN.

2) Network Architecture: PINNs are formulated to estimate the lame parameters of the material. Phantom data in 2D space (x,y) is given as input to the PINN network. The deep learning model consists of individual feed-forward neural networks to learn displacement and stress fields. From Equation (1), it can be observed that strain can be obtained by differentiating the displacement. Similarly, strain is obtained by differentiating the output from feed-forward neural networks. Equation (2) is used as the loss function to train the model which includes physics equations in addition to the data in its computations. The lame parameters of the material are considered as network parameters that change during the training phase.

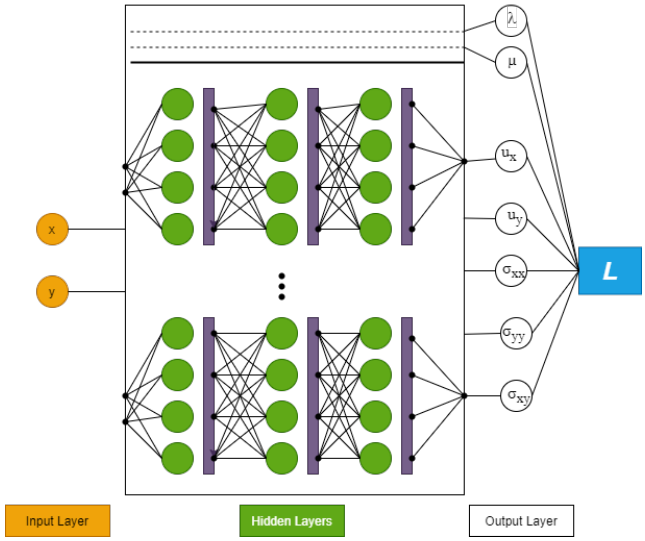

Fig. 2. Architecture of the PINN to estimate elastic properties of the tissue.

$$L = \begin{pmatrix} |u_x - u_x^*| + |u_y - u_y^*| \\ +|\sigma_{xx} - \sigma_{xx}^*| + |\sigma_{yy} - \sigma_{yy}^*| + |\sigma_{xy} - \sigma_{xy}^*| \\ +|(\lambda + 2\mu)\varepsilon_{xx} + \lambda\varepsilon_{xx} - \sigma_{xx}| \\ +|(\lambda + 2\mu)\varepsilon_{yy} + \lambda\varepsilon_{yy} - \sigma_{yy}| \\ +|2\mu\varepsilon_{xy} - \sigma_{xy}| \end{pmatrix} \tag{2}$$

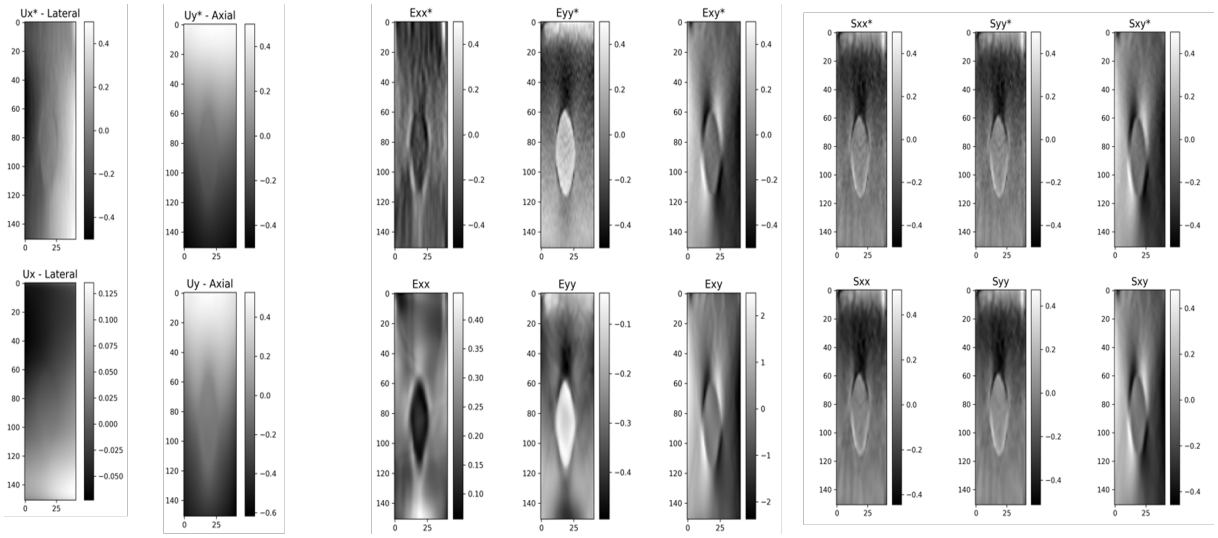

Fig. 3. First row corresponds to ground truth displacement, stress and strain of phantom obtained by using AM2D method [34]. Second row displays the outputs from the PINN.

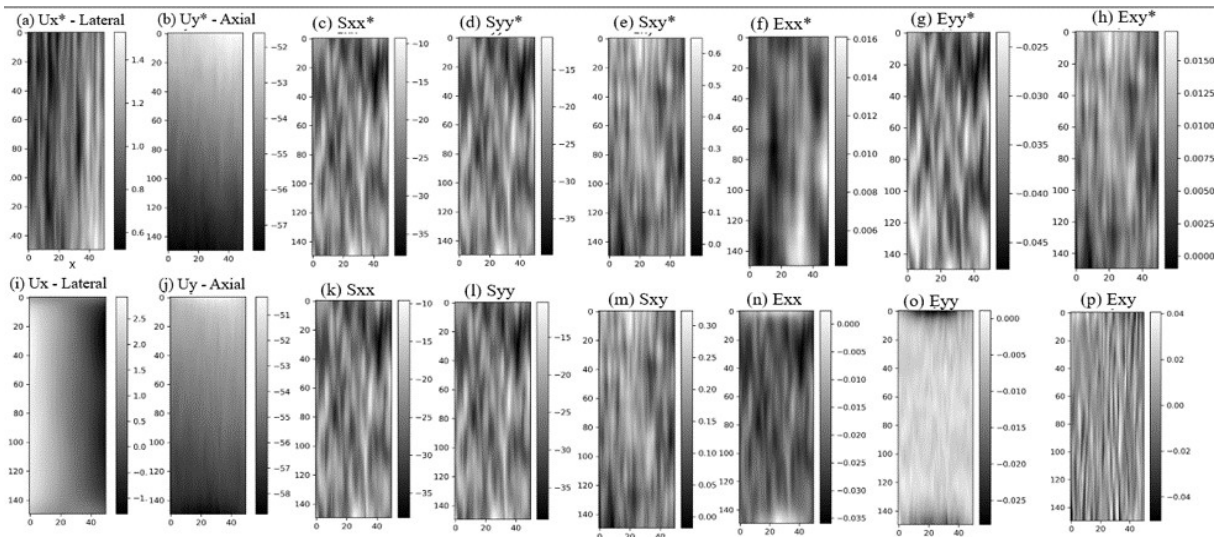

Fig. 4. (a-h) corresponds to ground truth (a) and (b) shows the lateral and the axial displacement of the lesion (c-e) correspond to the stress fields (f-h) displays the ground truth strain values (i-m) shows the displacement and stress values estimated by the feed-forward neural networks (n-p) displays the strain obtained by differentiating the outputs from feed-forward networks.

3) Model: The model has five independent feed-forward neural networks for displacement (u_x, u_y) and stress ($\sigma_{xx}, \sigma_{yy}, \sigma_{xy}$). Each feed-forward neural network has 50 layers with 10 neurons in each layer. Tanh activation function is used with 0.0001 as the learning rate. The loss function used to train the network is shown in Equation (2). λ and μ are considered as network parameters that change during the training phase.

III. Results and Discussion

During our initial experiments, the entire phantom data is given to the model to check whether the feed forward networks are learning the data properly or not. To facilitate the convergence of the model, the data is normalized in these experiments. The ground truth displacement, stress and strain of the whole dataset is displayed in the first row of Fig. 3. Second row in Fig. 3 shows the displacement and strain values learned by feed-forward neural networks which are used to compute the stress. From the figures, it can be observed that the model was doing a decent job in learning the input data provided to it. But, as the input data consists of two materials (lesion and background), the model was not able to predict the lame constant values properly. In order to solve this problem, only lesion data was extracted and was fed to the model without any normalization as shown in Fig. 4. The model converged properly and was able to predict λ value close to ground truth. The ground truth λ value is 920 kPa whereas the value predicted by the model is 925.319 kPa.

IV. Conclusion

In this paper, we proposed a PINN-based approach to solve inverse problems in the domain of ultrasound elastography. The model took pre and post compression images of a phantom as input and estimated one of the lame constants (λ) of the material. In contrast to typical deep learning models, the training of this model converges using a small amount of data. From the results, it can be observed that the λ value predicted by the model is quite close to the ground truth value. Our future work will focus on experimenting with new data sets and using advanced deep learning network architectures to predict both lame constants of a given material accurately with minimal amount of data.

References

[1] S. Srinivasan, T. Krouskop, and J. Ophir, "A quantitative comparison of modulus images obtained using nanoindentation with strain elastograms," *Ultrasound in medicine & biology*, vol. 30, no. 7, pp. 899–918, 2004.

[2] Y. Fu, C. Chui, C. Teo, and E. Kobayashi, "Elasticity imaging of biological soft tissue using a combined finite element and non-linear optimization method," *Inverse Problems in Science and Engineering*, vol. 23, no. 2, pp. 179–196, 2015.

[3] S.-H. Lee and D. Terzopoulos, "Heads up! biomechanical modeling and neuromuscular control of the neck," *ACM SIGGRAPH 2006 Papers*, 2006, pp. 1188–1198.

[4] S. Sueda, A. Kaufman, and D. K. Pai, "Musculotendon simulation for hand animation," *ACM SIGGRAPH 2008 papers*, 2008, pp. 1–8.

[5] Á. Takács, I. J. Rudas, and T. Haidegger, "Surface deformation and reaction force estimation of liver tissue based on a novel nonlinear mass–spring–damper viscoelastic model," *Medical & biological engineering & computing*, vol. 54, no. 10, pp. 1553–1562, 2016.

[6] K. Erleben, J. Sporring, and H. Dohlmann, "Opentissue-an open source toolkit for physics-based animation," *MICCAI Open-Source Workshop*, vol. 3, 2005.

[7] D. M. McGrath, W. D. Foltz, A. Al-Mayah, C. J. Niu, and K. K. Brock, "Quasi-static magnetic resonance elastography at 7 t to measure the effect of pathology before and after fixation on tissue biomechanical properties," *Magnetic resonance in medicine*, vol. 68, no. 1, pp. 152–165, 2012.

[8] A. Erdemir, M. L. Viveiros, J. S. Ulbrecht, and P. R. Cavanagh, "An inverse finite-element model of heel-pad indentation," *Journal of biomechanics*, vol. 39, no. 7, pp. 1279–1286, 2006.

[9] K. Liu, M. R. VanLandingham, and T. C. Ovaert, "Mechanical characterization of soft viscoelastic gels via indentation and optimization-based inverse finite element analysis," *Journal of the Mechanical Behavior of Biomedical Materials*, vol. 2, no. 4, pp. 355–363, 2009.

[10] D. Mojsejenko, J. R. McGarvey, S. M. Dorsey, J. H. Gorman, J. A. Burdick, J. J. Pilla, R. C. Gorman, and J. F. Wenk, "Estimating passive mechanical properties in a myocardial infarction using mri and finite element simulations," *Biomechanics and modeling in mechanobiology*, vol. 14, no. 3, pp. 633–647, 2015.

[11] B. Rebholz, F. Zheng, and M. Almekkawy, "Two-dimensional iterative projection method for subsample speckle tracking of ultrasound images," *Medical & Biological Engineering & Computing*, vol. 58, no. 12, pp. 2937–2951, 2020.

[12] M. K. Almekkawy, Y. Adibi, F. Zheng, E. Ebbini, and M. Chirala, "Two-dimensional speckle tracking using zero phase crossing with riesz transform," *Proceedings of Meetings on Acoustics 168ASA*, vol. 22, no. 1. Acoustical Society of America, 2014, p. 020004.

[13] M. Almekkawy and E. Ebbini, "Two-dimensional speckle tracking using parabolic polynomial expansion with riesz transform," *2017 IEEE 14th International Symposium on Biomedical Imaging (ISBI 2017)*. IEEE, 2017, pp. 201–205.

[14] B. Rebholz and M. Almekkawy, "Constrained rf level interpolation for normalized cross correlation based speckle tracking," *2020 IEEE International Ultrasonics Symposium (IUS)*. IEEE, 2020, pp. 1–4.

[15] B. Rebholz and M. Almekkawy, "Analysis of speckle tracking methods: Correlation and rf interpolation," *2020 IEEE 4th International Conference on Image Processing, Applications and Systems (IPAS)*. IEEE, 2020, pp. 120–124.

[16] B. Rebholz and M. Almekkawy, "Efficacy of kriging interpolation in ultrasound imaging; subsample displacement estimation," *2020 42nd Annual International Conference of the IEEE Engineering in Medicine & Biology Society (EMBC)*. IEEE, 2020, pp. 2137–2141.

[17] S. Bharadwaj, S. Prasad, and M. Almekkawy, "An upgraded siamese neural network for motion tracking in ultrasound image sequences," *IEEE Transactions on Ultrasonics, Ferroelectrics, and Frequency Control*, 2021.

[18] S. Bharadwaj and M. Almekkawy, "Faster search algorithm for speckle tracking in ultrasound images," *2020 42nd Annual International Conference of the IEEE Engineering in Medicine & Biology Society (EMBC)*. IEEE, 2020, pp. 2142–2146.

[19] S. Bharadwaj and M. Almekkawy, "Deep learning based motion tracking of ultrasound image sequences," *2020 IEEE International Ultrasonics Symposium (IUS)*. IEEE, 2020, pp. 1–4.

[20] S. Bharadwaj and M. Almekkawy, "Improved siamese network for motion tracking in ultrasound images," *The Journal of the Acoustical Society of America*, vol. 149, no. 4, pp. A114–A114, 2021.

[21] S. Bharadwaj and M. Almekkawy, "Motion estimation for ultrasound image sequences using deep learning," *The Journal of the Acoustical Society of America*, vol. 148, no. 4, pp. 2487–2487, 2020.

[22] M. Svensén and C. M. Bishop, "Pattern recognition and machine learning," 2007.

[23] Y. LeCun, Y. Bengio, and G. Hinton, "Deep learning," *nature*, vol. 521, no. 7553, pp. 436–444, 2015.

[24] Y. Bengio, I. Goodfellow, and A. Courville, *Deep learning*. MIT press Massachusetts, USA:, 2017, vol. 1.

[25] M. Raissi, P. Perdikaris, and G. E. Karniadakis, "Physics-informed neural networks: A deep learning framework for solving forward and inverse problems involving nonlinear partial differential equations," *Journal of Computational Physics*, vol. 378, pp. 686–707, 2019.

[26] M. Raissi, A. Yazdani, and G. E. Karniadakis, "Hidden fluid mechanics: Learning velocity and pressure fields from flow visualizations," *Science*, vol. 367, no. 6481, pp. 1026–1030, 2020.

[27] E. Haghighat, M. Raissi, A. Moure, H. Gomez, and R. Juanes, "A deep learning framework for solution and discovery in solid mechanics," *arXiv preprint arXiv:2003.02751*, 2020.

[28] M. Yin, X. Zheng, J. D. Humphrey, and G. E. Karniadakis, "Non-invasive inference of thrombus material properties with physics-informed neural networks," *Computer Methods in Applied Mechanics and Engineering*, vol. 375, p. 113603, 2021.

[29] Y. Chen, L. Lu, G. E. Karniadakis, and L. Dal Negro, "Physics-informed neural networks for inverse problems in nano-optics and metamaterials," *Optics express*, vol. 28, no. 8, pp. 11 618–11 633, 2020.

[30] G. Pang, L. Lu, and G. E. Karniadakis, "fpinns: Fractional physics-informed neural networks," *SIAM Journal on Scientific Computing*, vol. 41, no. 4, pp. A2603–A2626, 2019.

[31] L. Yang, D. Zhang, and G. E. Karniadakis, "Physics-informed generative adversarial networks for stochastic differential equations," *arXiv preprint arXiv:1811.02033*, 2018.

[32] L. Yang, X. Meng, and G. E. Karniadakis, "B-pinns: Bayesian physics-informed neural networks for forward and inverse pde problems with noisy data," *Journal of Computational Physics*, vol. 425, p. 109913, 2021.

[33] E. Haghighat and R. Juanes, "Sciann: A keras/tensorflow wrapper for scientific computations and physics-informed deep learning using artificial neural networks," *Computer Methods in Applied Mechanics and Engineering*, vol. 373, p. 113552, 2021.

[34] H. Rivaz, E. M. Boctor, M. A. Choti, and G. D. Hager, "Real-time regularized ultrasound elastography," *IEEE transactions on medical imaging*, vol. 30, no. 4, pp. 928–945, 2010.